HEAT and TECHNOLOGY
CALOR e TECNOLOGIA
Vol. 3 • No. 1 • 1985

EXPERIMENTAL ANALYSIS OF THE VELOCITY FIELD IN AN ANNULAR CHANNEL WITH ELICOIDAL WIRE

Marcelo José Santos de Lemos (*), Pedro Carajilescov (**)

ABSTRACT

In general, nuclear reactor fuel elements are rod bundles with coolant flowing axially among them. LMFBR's (Liquid Metal Fast Breeder Reactor) have wire wrapped fuel rods, with the wire working as spacer and mixer. The present work consists in the experimental analysis of the velocity field created by a typical LMFBR fuel rod placed in a cylinder, yielding an annular channel with helicoidal wire. Using hot wire anemometry, the main and secondary velocity fields were measured. The range for Re was from 2.2×10^4 to 6.1×10^4, for air. The aspect ratio, P/D, and the lead-to-diameter ratio, ℓ/D, were 1.2 and 15, respectively.

INTRODUCTION

Nuclear reactor fuel elements generally consist of rod bundles where fuel pellets in cylindrical form are encapsulated in cladding tubes. The coolant flowing axially among the rods,

(*) Mechanical Engineering Department Pontifícia Universidade Católica do Rio de Janeiro, Rio de Janeiro, Brazil. Presently at Argonne National Laboratory, Illinois, USA.

(**) Instituto Tecnológico da Aeronáutica, CTA, São José dos Campos, São Paulo, Brazil.

extracts heat and transports it to a turbine in order to produce mechanical energy.

The thermalhydraulic analysis of fuel elements is of importance to improve design criteria regarding safety, thermal eficiency, initial and maintenance costs, etc. Therefore, the determination of the velocity and temperature fields, mixing, cross-flow rates, and friction factor, are important tasks in core thermal design.

The flow through Light Water Reactor rod bundles has been extensively investigated in the literature, as for example in [1,2]. Fast reactors such as LMFBR, however, have wire wrapped rods with the wire working as spacer and mixer. A schematic is shown in Figure 1.

Among many experimental works using this geometry, one can mention Lafay [3], who measured the static pressure distribution in a 19-rod element external wall and the velocity in the peripheral region using bubble visualization technique. Fernandez [4] measured the static pressure distribution and rod wall shear stress in a 7-pin assembly.

The complexity of the velocity field in such geometries increases the difficulty in interpreting the results, since there is the influence of the field created by a typical rod with the fields generated by the others. In addition, Lafay [3] showed that the observed high cross-flow is the predominant energy exchange mechanism among channels.

The present work consisted in the experimental analysis of the axial and transverse velocity fields created by a typical LMFBR fuel rod placed in a cylinder yielding an annular channel with helicoidal wire. The purpose of using this geometry is to investigate the generated flow field free of interference from the other rods. The Re range was from 2.2×10^4 to 6.1×10^4.

EXPERIMENTAL FACILITY

Apparatus

The experimental apparatus used is schematically shown in

Figure 2, and basically consists of an air blowing section and a test section,coupled in an open loop configuration.

Air enters the circuit through a centrifugal fan. The mass flow rate desired was controlled by a by-pass valve located downstream the fan exit, so that the fan operated always at full power. A honey-comb was inserted after the by-pass in order to homogenize the flow. The piping connecting the fan and the plenum had an internal diameter equal to 12,7 cm and was 2400 cm long. On the pipe wall, were mounted a Pitot Static Tube and a platinum resistance thermometer.

Another honey-comb cell was located in the plenum entrance to reduce secondary flows induced by the pipe elbow. The plenum had a cross-section area 31 times greater than the pipe cross-section area.

Preliminary tests indicated that the system temperature reached steady state after 20 minutes from start up.

The test section simulated the flow around a typical LMFBR fuel rod. A 5 to 1 enlargement in the actual design dimensions was used to facilitate instrumentation instalation and to improve measuring accuracy. A schematic is shown in Figure 3. The main parameters are: $P/D = 1/2$, $\ell/D = 15$, $L/D_h = 141$, where D is the rod diameter, P the rod pitch in a triangular lattice, ℓ the wire lead length, and D_h the wetted perimeter referent to the annulus cross-section.

Instrumentation

The air blowing section was set up with a Mettler TM16 platinum resistance thermometer used to monitor the test section inlet bulk temperature. This section also had a pitot tube for initial mass flow estimates.

The test section was used for measuring pressure loss and flow velocity in the channel.

The static pressure taps, in a total of 13, were installed in the outside tube wall following a helicoidal path of the same lead length as the test section helix. This was done to obtain pressure losses along the flow streamlines.

The velocity measuring technique used was hot-wire anemometry. The measurement system was composed by a signal processor and a probe translation mechanism.

The signal processor consisted of a TSI anemometer and probe. The probe model 1210 TSI was repaired with 6μ tungsten wire with the help of a DISA55 A 11 Micromanipulator and a DISA55 A 12 Welding Power Generator Unit. The enlargement required for the operation was obtained with a ZEISS stereomicroscope. The probe was connected to a 1050 TSI Constant Temperature Anemometer. The signal was then passed through a 1052 TSI Linearizer and a 1057 TSI Signal Conditioner. A digital voltmeter model 8000A FLUKE was used to read the output voltage. A block diagram is shown in Figure 4.

The hot-wire probe was installed inside a transversing mechanism fixed at $118D_h$ downstream the test section inlet. This mechanism provided radial positioning only, and it is shown in Figure 5. The probe was inserted in a sliding tube which was coupled to a micrometer. This mechanism allowed easy probe substitution as well as adjustment in the sensor angular position. The initial measuring position was the internal wall surface and it was indicated by means of electrical contact of probe prongs and the steel rod. The probe angular displacement was obtained by rotating manually the movable rod instead of rotating the probe. The rod rotation is shown in Figure 6.

RESULTS AND DISCUSSION

Velocities

The velocity components were measured by placing the sensor into two different attack angles, according to Figure 7. The two angles were chosen in such a way that one had always the sensor approximately inclined 45^o relative to the streamwise flow direction. This fact enabled the measurement of velocities large compared to expected turbulent components. In addition, lateral wire cooling effects were minimized in both positions. A previous study had shown that for the probe used, angles of attack less

than 45^{o} did not cause detectable measuring errors due to the cooling effect of components aligned with the sensor.

The two obtained velocities were called U_{33} and U_{57}. The axial velocity U_x, and the tangencial velocity, U_θ were calculated as follows,

$$U_x = U_{33} \cos(33^{o}) + U_{57} \cos(57^{o})$$

and

$$U_\theta = - U_{33} \sin(33^{o}) + U_{57} \sin(57^{o})$$

The components were nondimensionalized through the mean velocity,defined as,

$$\overline{U}_x = \frac{1}{A} \int_A U_x \, dA$$

where A is the annular channel cross-section area.

Figures 8-9 show radial distribution of U_x for several angles θ. The results are plotted against the ordinate y, defined as,

$$y = \frac{r - r_1}{r_2 - r_1}$$

where r is the radius of measurement, r_1 and r_2 are the internal and external gap radii, respectively. The figures indicate that the higher the angle θ, which measures the probe angular position, the lower the axial velocity. Also, the profile shapes are kept roughly the same. The Reynolds number influence, shown in Figures 10-11, is verified by the profiles flattening as Re increases, although the Re range measured was not large enough for definite conclusions to be drawn. The profile flattening along the radial direction is shown by the velocity decrease near the channel center region and by the velocity increase near the wall regions, as Re increases.

The tangencial component, U_θ, is shown in Figures 12-13. Results are on the average 24% of U_x. The expected ratio would be

$$\frac{U_\theta}{U_x} = \frac{1}{tg\ \alpha}$$

where α is the angle made by the tangent to the helix and the channel axis. For $\ell/D = 15$, U_θ should account for only 21% of U_x. This difference can be explained as due to uncertainties in the hot-wire angular position and due to secondary flow. The figures suggest that the point of maximum velocity approaches the outside wall as θ increases. This fact is due to the fluid rotation induced by the wire, pushing the fluid against the outside tube. The variation of Re, within the range studied, did not affect substantially U_θ, as seen in Figures 14-15.

Secondary Flow

With the help of Figure 3, one can define the directions η and ξ as directions along and perpendicular to the helix, respectively. For the fully developed region, the parameters characterizing the flow, with exception of pressure, shall not change along the η coordinate. Therefore, one can consider the flow component in the ξ direction as the secondary flow. The velocity U_ξ is given by,

$$U_\xi = U_\theta \sin \alpha - U_x \cos \alpha$$

The continuity equation written for a general surface is,

$$\int_{\text{Surface}} \rho \vec{U} \cdot d\vec{A} = 0$$

For a surface formed by the η and radial directions, perpendicular to ξ, the above equation gives,

$$\int_{r_1}^{r_2} U_\xi \, dr = 0$$

However, when calculated numerically, this condition was not satisfied. The reasons for this discrepancy are two. First, uncertainties in the sensor angular positioning, and second, uncertainties associated with the accuracy of the helix angle due to manufacturing difficulties.

The velocity U_ξ was then assumed to be,

$$U_\xi = U_\theta \sin(\alpha + \Delta\alpha) - U_x \cos(\alpha + \Delta\alpha)$$

where $\Delta\alpha$ accounts for those difficulties.The value of $\Delta\alpha$ was numerically adjusted such that the continuity equation was satisfied, for each angular position. Its value did not exceed 5^o. Figure 16 shows U_ξ distributions.

Since this component is on the average small compared to the turbulent velocity components of the flow, the data are quite spread. Nevertheless, a few remarks can be said based upon the sistematic behaviour of the experimental points. The maximum value for U_ξ is around 5% of $\overline{U}_x$ for $\theta = 300^o$. Figure 16 also suggests the existence of two secondary flow loops, as roughly pictured in Figure 17. It was also observed that this component is not significantly affected by the Reynolds number variation.

Friction Factor

The test section pressure losses were referred to the plenum and were measured along the helix. They are presented in the nondimensional form, $\Delta P/\rho\ \overline{U}_x^2/2g_c$, where ΔP is the pressure differential between the axial position x and the plenum, ρ the air density, $\overline{U}_x$ the mean axial velocity and g_c a conversion factor. The results for different streamlines (different θ) and Re = 22600 are shown in Figure 18. The figure shows that, for the geometry used, the static pressure did not vary considerably with the angle θ. This could be atributed to the poor manometer sensitivity. The data also indicate that the flow can be considered fully developed ($\Delta P/\Delta x$ = constant) for x/D_h higher than 30.

The friction factor, defined as,

$$f = \frac{\Delta P}{\Delta x} \quad \frac{D_h}{\frac{2\rho \overline{V}_x^2}{g_c}}$$

is calculated for the fully developed region and presented in Figure 19, compared with results for pipes and annular channels [5]. The present data are lower than the f given by Blasius formula and the one measured by Brigton & Jones [5].In [5],the ratio P/D is greater than the one used in the present work.

Error Analysis

The error analysis for the measurements here presented was based upon consideration of two factors: the error due to signal processing system and the error due to sensor positioning.

Assuming that the signal processing error, e_s, could be considered as a deterministic factor and divided as,

$$e_s = e_a + e_u + e_v$$

where e_a is the anemometer error, e_u the linearizer error and e_v the voltmeter error, the total error, e_s, was calculated using manufacturer's data and found to be less than 4.85%.

The sensor angular positioning had a uncertainty of $\pm 5^o$. This caused an estimated error of 2,2% for the axial velocity U_x, and 10.5% for the tangencial velocity U_θ.

Comments

The extrapolation of the results here presented to the analysis of LMFBR fuel assemblies can be obtained by geometrically combining the velocity vectors in different angular positions, according to the disposition of the rods inside the element. This idea is shown in Figure 20.

By means of this model, one can have the cross-flow rates at the boundaries of each subchannel. Having this information at the subchannel boundary, there is no need to solve the transverse

momentum equation in addition to the axial momentum equation in order to describe the flow field. The solution of the transverse momentum equation in subchannel analysis is known to constitute a drawback in most computer codes which use this method.

As a suggestion for further experimental work, one can mention the measurement of the full field in a bundle and comparisons with the vector composition mentioned above. The results can lead to improvements in LMFBR fuel assemblies design.

ACKNOWLEDGEMENT

The first author wishes to thank Comissão Nacional de Energia Nuclear - CNEN, Brazil, for financial support during the preparation of this work.

NOMENCLATURE

Name	Dimensions/Units
A = Annular channel cross section area	1732.30 mm^2
D = Rod diameter	50.80 mm
D_2 = Tube internal diameter	69.85 mm
D_3 = Tube external diameter	73.00 mm
D_h = Test section hydraulic diameter	17.0 mm
e_a = Anemometer reading error	
e_v = Voltmeter reading error	
e_u = Linearizer reading error	
e_s = Total measuring error	
f = Friction factor	
ℓ = wire lead length	mm
L = Test section length	2400 mm
L_m = Probe location related to the test section inlet	2000 mm
P = Pressure	
P = Rod pitch	mm
U_{33} = Velocity component in the first measuring position	m/s
U_{57} = Velocity component in the second measuring position	m/s
U_x = Velocity component in the axial direction	m/s
U_θ = Velocity component in the tangencial direction	m/s
$\overline{U}_x$ = Mean axial velocity	m/s

U_η = Velocity component in the η direction m/s
U_ξ = Velocity component in the ξ direction m/s
x = Axial coordinate m
y = Nondimensional radial coordinate
θ = Angle measuring probe angular displacement degree
η = Direction tangent to helix
ξ = Direction perpendicular to helix
R_e = Reynolds number

REFERENCES

1. A.C. Trupp: The structure of Turbulent Flow in Triangular Array Rod Bundles, Ph.D. Thesis, Mech. Eng. Department, University of Manitoba, Canada (1973).

2. P. Carajilescov, N.E. Todreas: Experimental and Analytical Study of Axial Turbulent Flow in an Interior Subchannel of Bare Rod Bundle, ASME Publication 75-WA/HT-51 (1976).

3. J. Lafay, B. Menant, J. Barroil: Local Pressure Measurements and Peripheral Flow Visualization in a Water 19-Rod Bundle Compared with FLICA II B Calculations - Influence of Helical Wire-Wrap Spacer System, Proceedings of the Meeting on the Liquid Metal Boiling Working Group, Risley, U.K, CEA-CONF-3491 (1975).

4. E.F. Fernandez: Estudo Experimental das Distribuições da Pressão Estãtica e da Tensão Cisalhante Superficial em um Feixe de Sete Barras com Espaçadores Helicoidais, M.Sc. Thesis, Pontifícia Universidade Catõlica do Rio de Janeiro, DEM-PUC/RJ, Rio de Janeiro (1978).

5. J.A. Brighton, J.B. Jones: Fully Developed Turbulent Flow in Annuli, J. of Basic Engineering, Vol. 9, pp, 835 (1964).

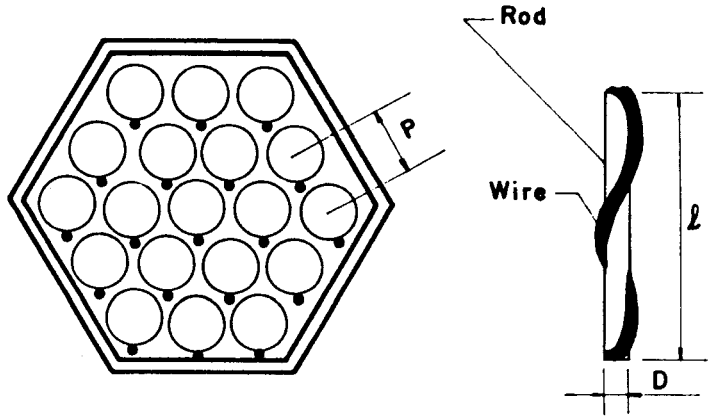

FIG. 1 - LMFBR 19-ROD FUEL ELEMENT GEOMETRY

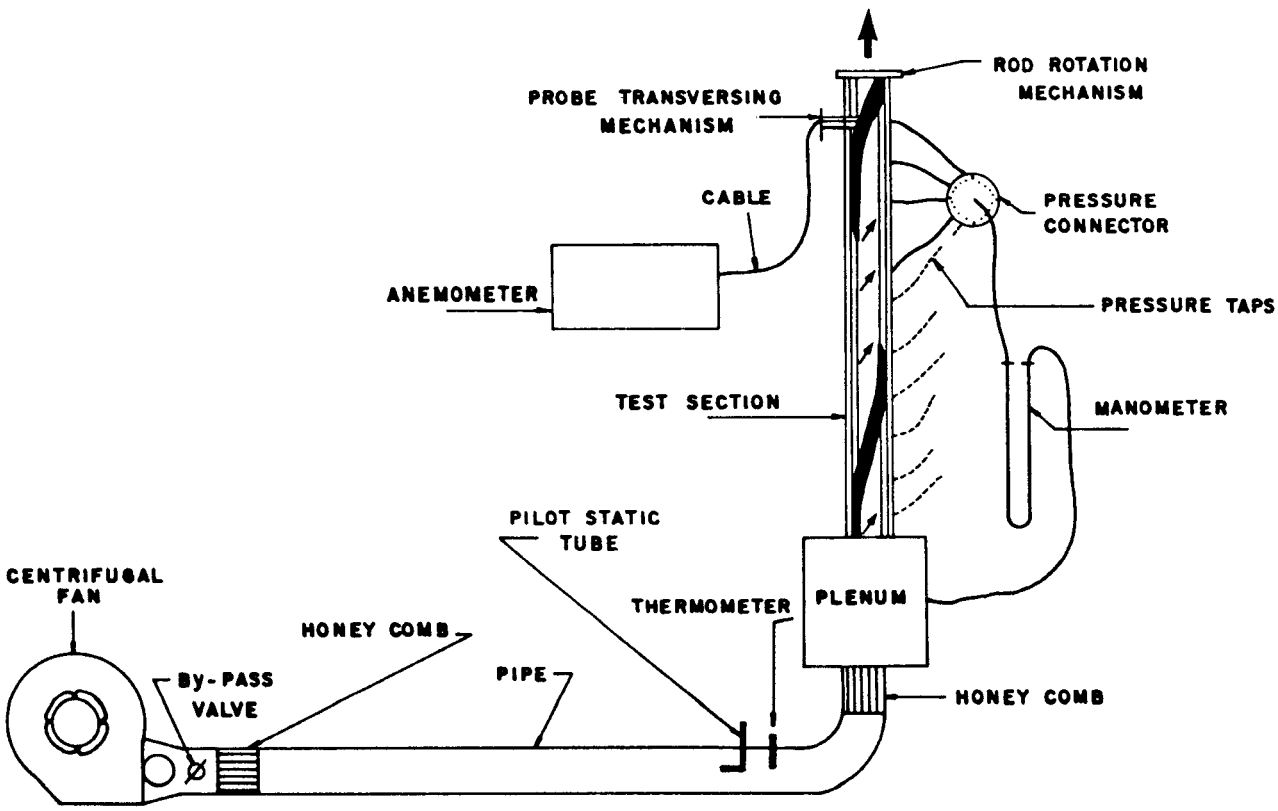

FIG. 2 - EXPERIMENTAL APPARATUS

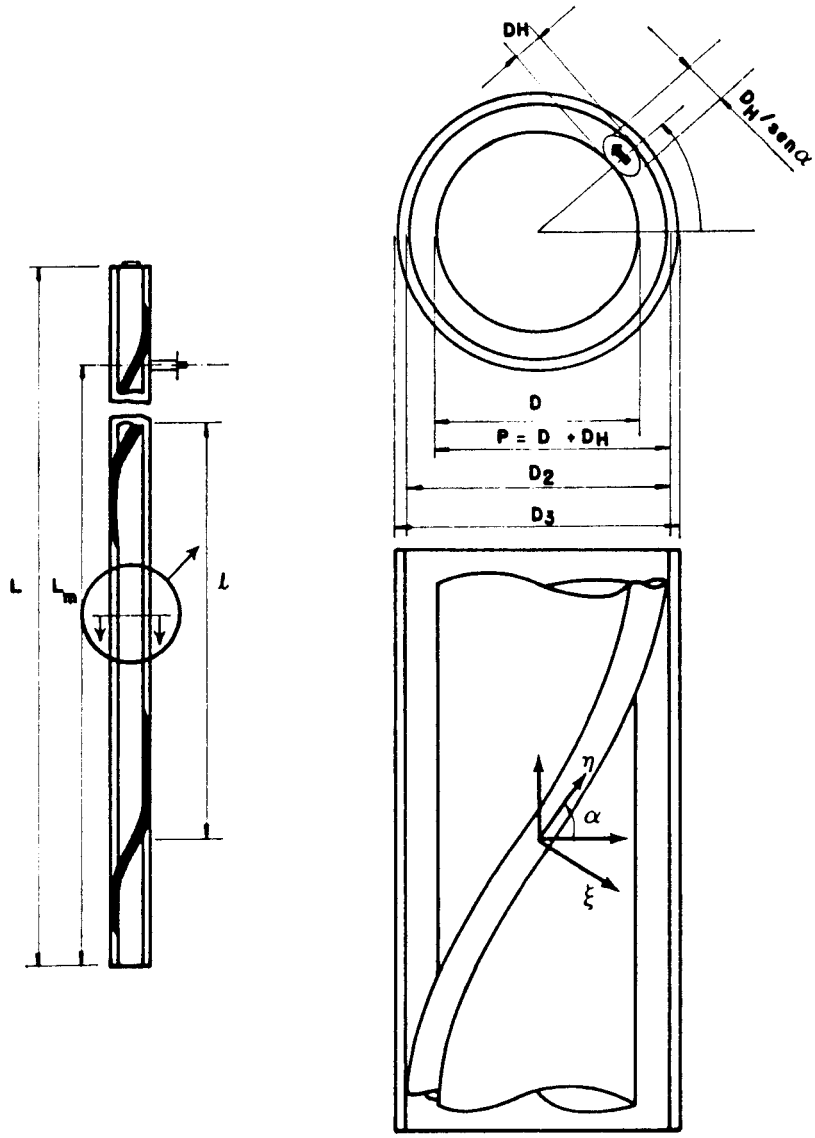

FIG. 3 - TEST SECTION

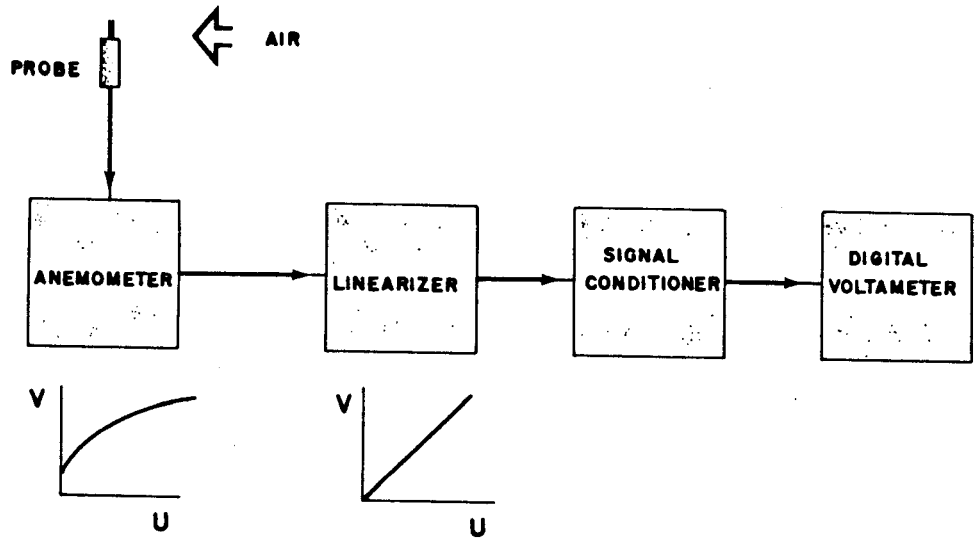

FIG. 4 - BLOCK DIAGRAM OF ANEMOMETRIC SYSTEM

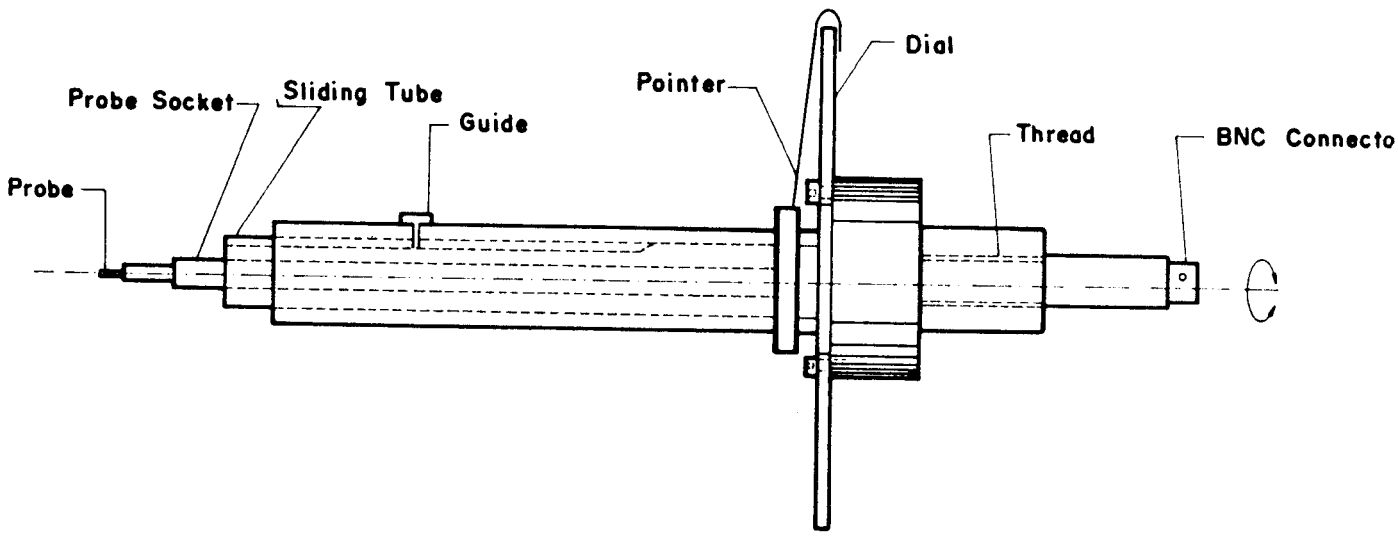

FIG. 5 - PROBE TRANSVERSING MECHANISM

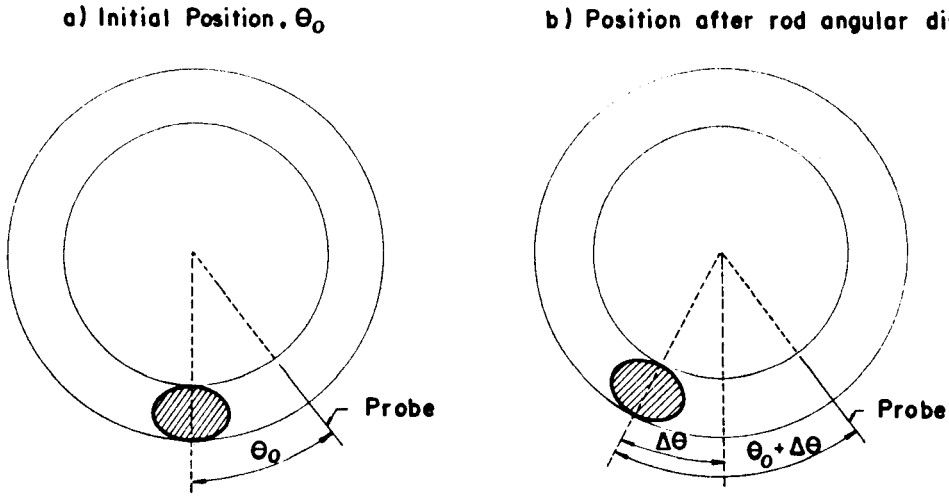

FIG. 6 - PROBE ANGULAR DISPLACEMENT

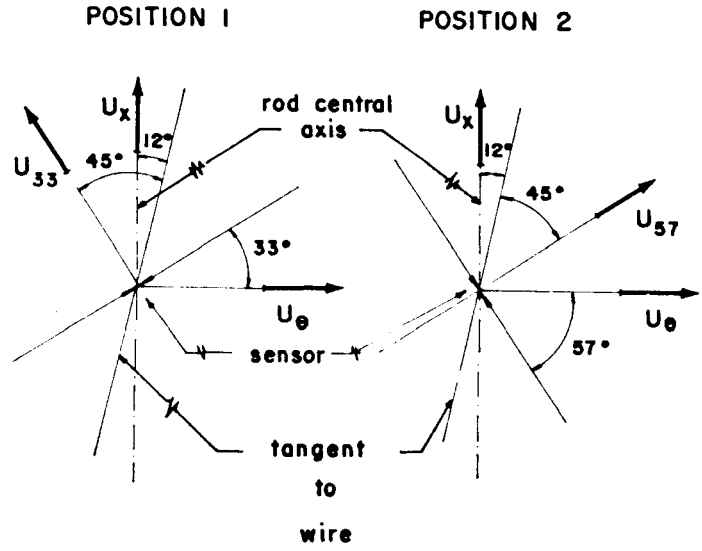

FIG. 7 - PROBE ANGULAR POSITIONING

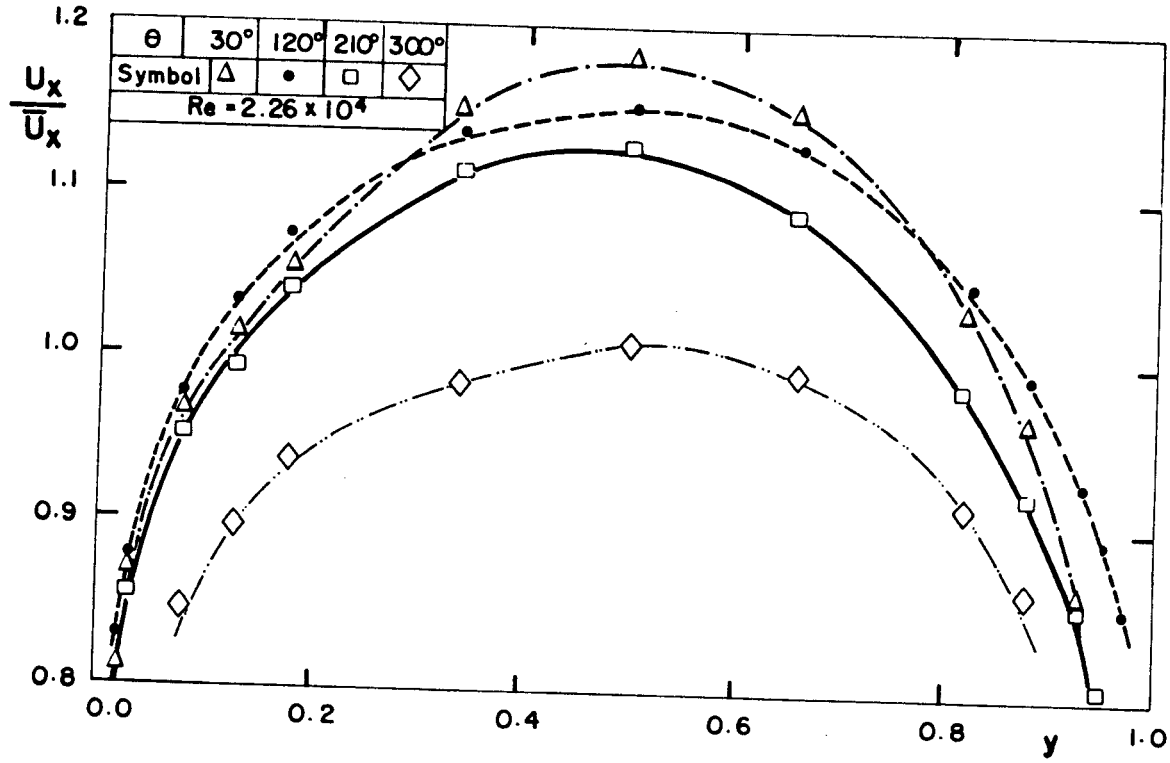

FIG. 8 - AXIAL VELOCITY DISTRIBUTION, Re = 22 600

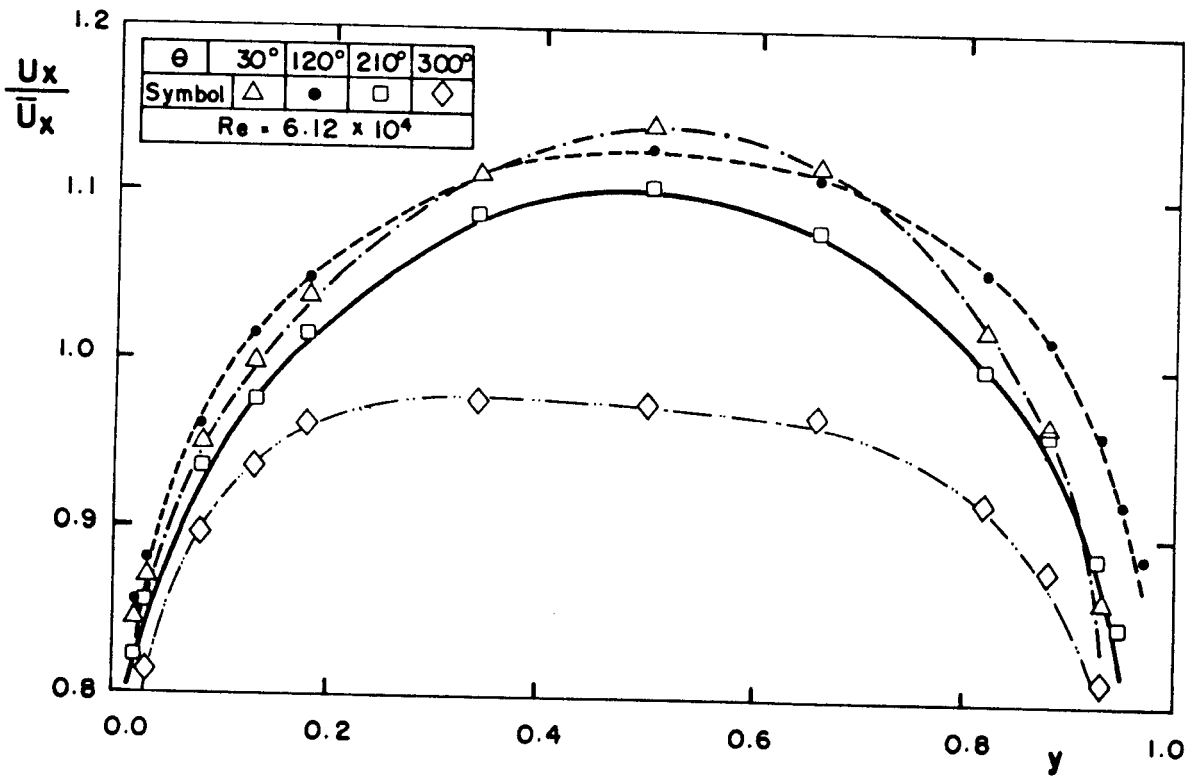

FIG. 9 - AXIAL VELOCITY DISTRIBUTION, Re = 61 200

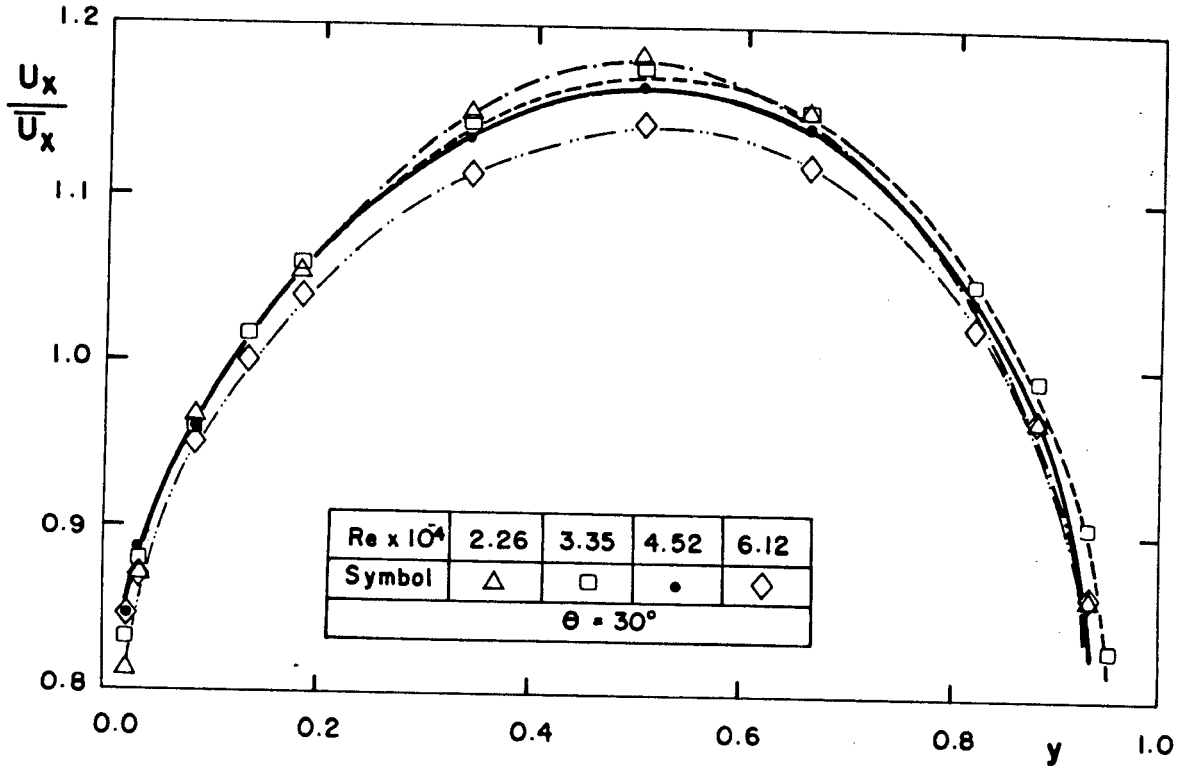

FIG. 10 - AXIAL VELOCITY DISTRIBUTION , θ = 30°

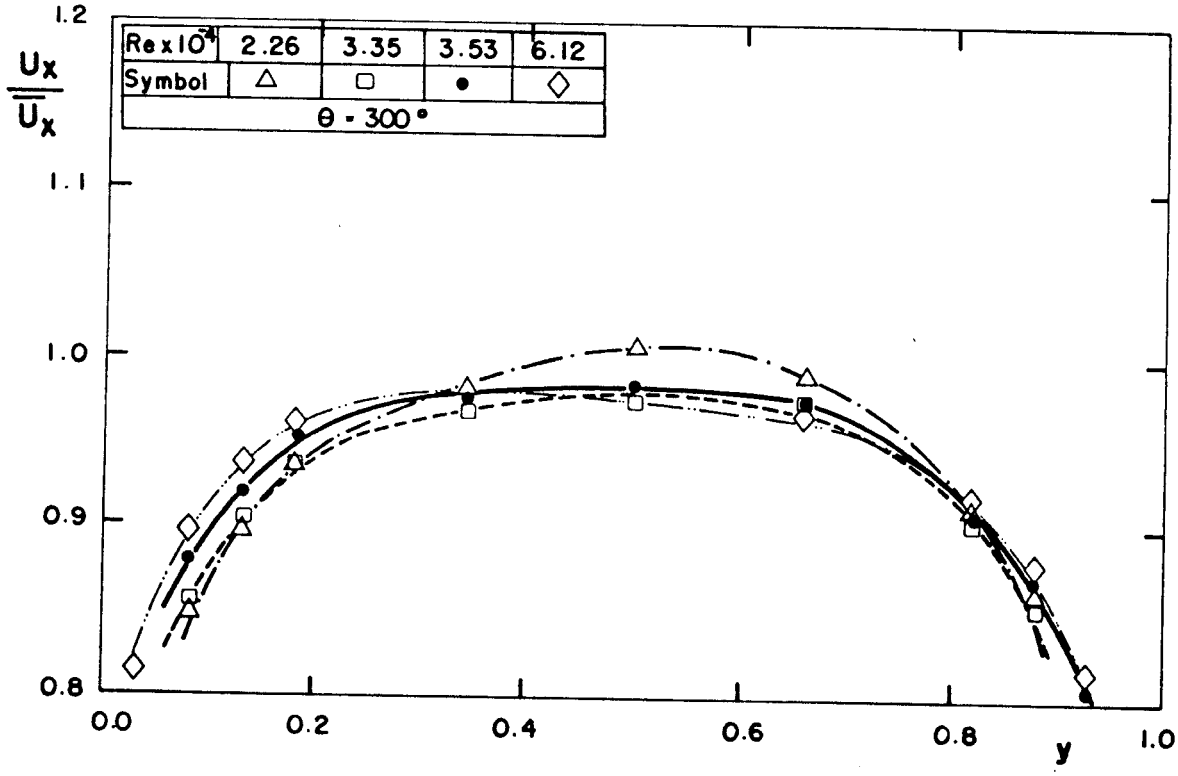

FIG. 11 - AXIAL VELOCITY DISTRIBUTION θ = 300°

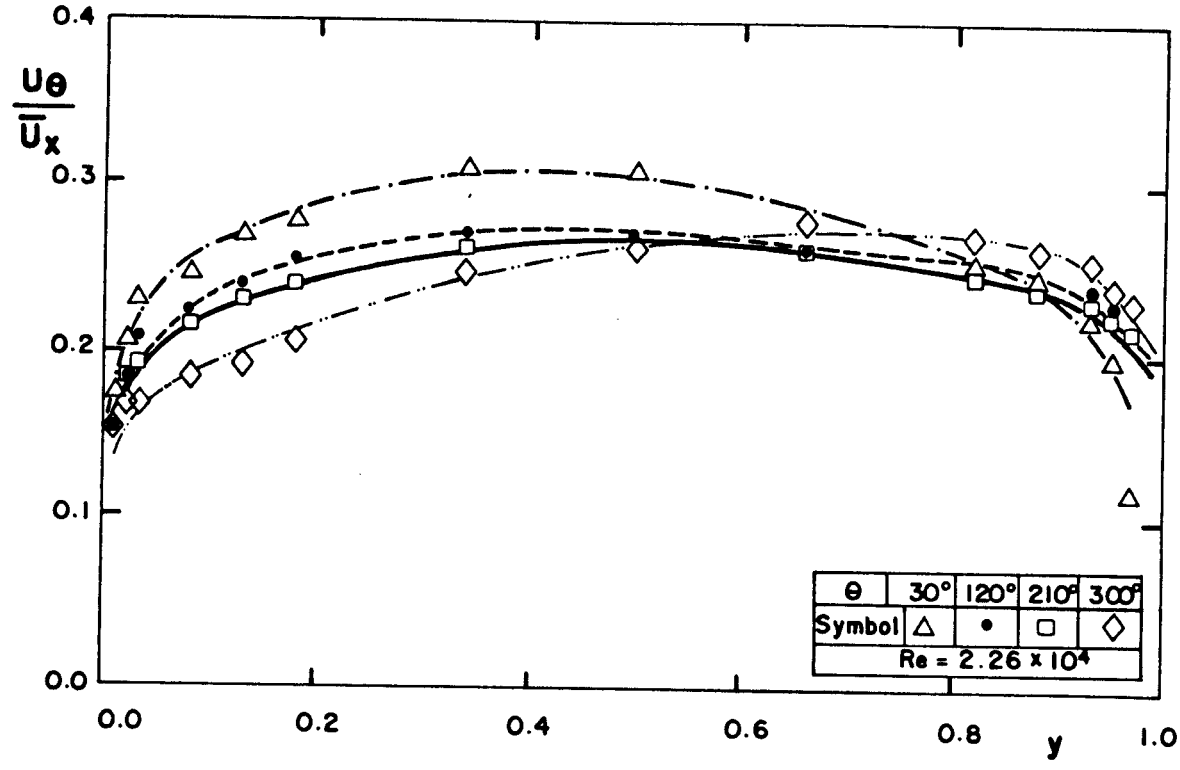

FIG. 12 - TANGENCIAL VELOCITY DISTRIBUTION , Re = 22 600

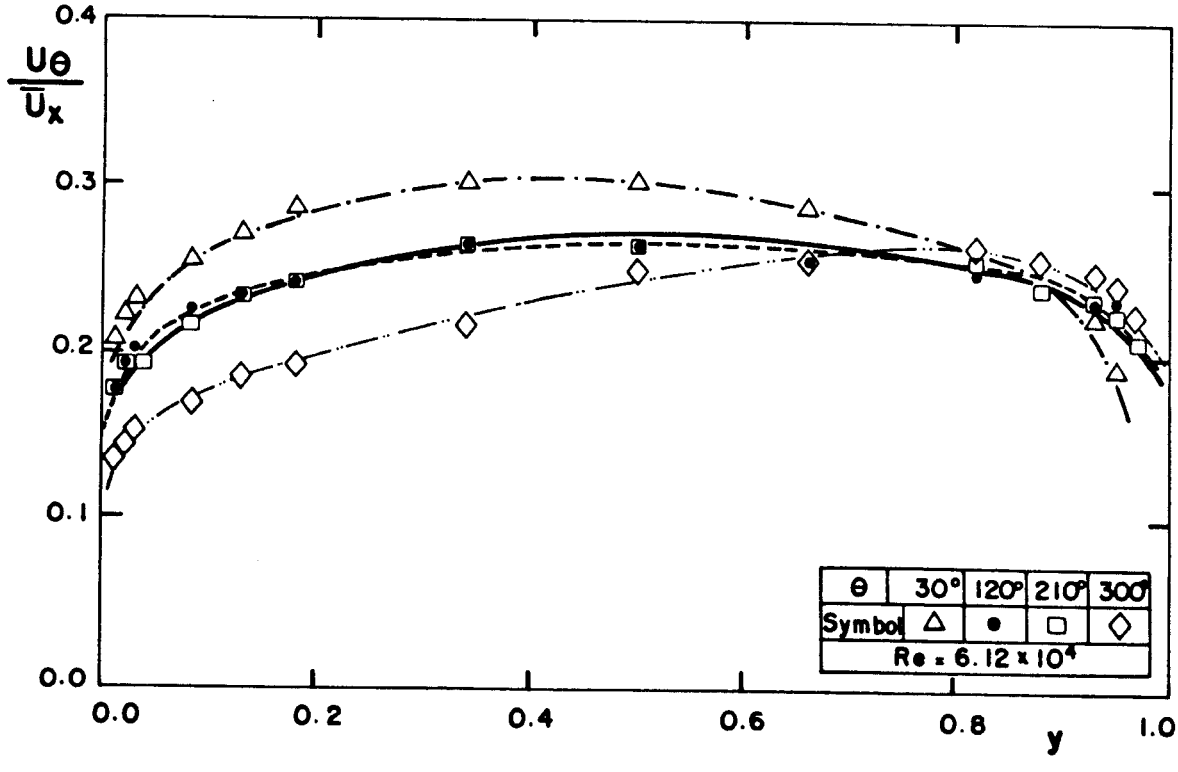

FIG. 13 - TANGENCIAL VELOCITY DISTRIBUTION , Re = 61 200

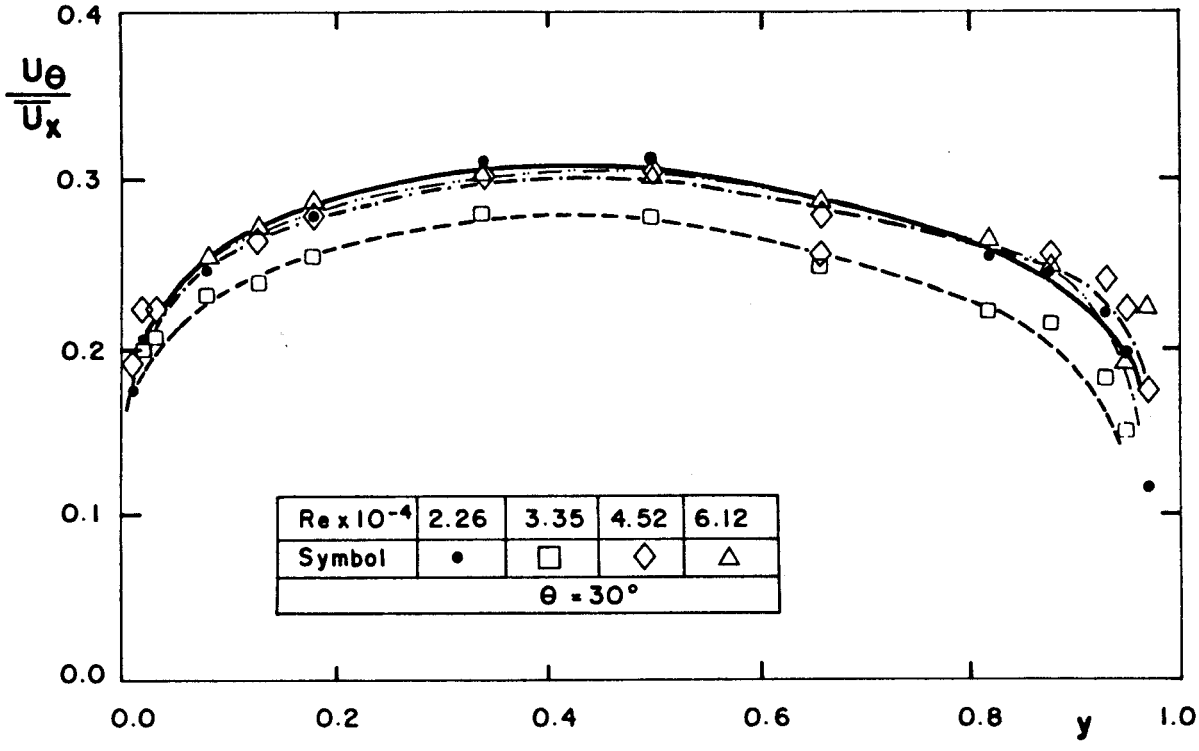

FIG. 14 - TANGENCIAL VELOCITY DISTRIBUTION , θ = 30°

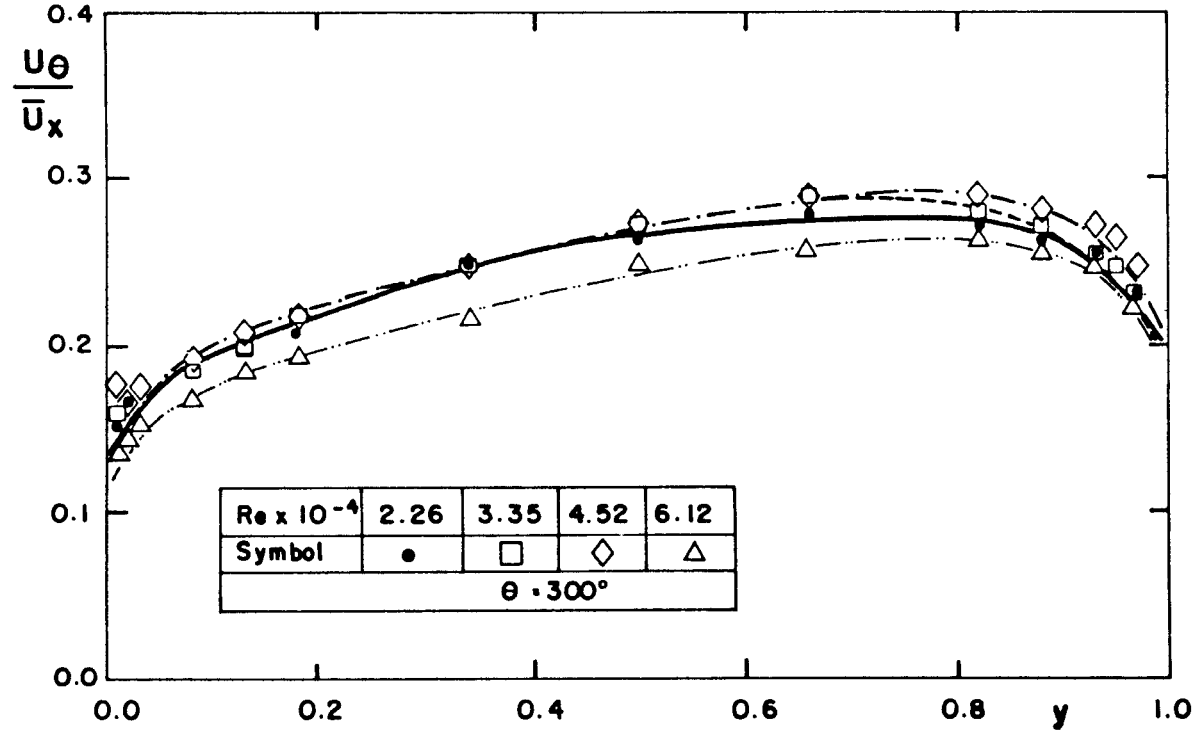

FIG. 15 - TANGENCIAL VELOCITY DISTRIBUTION , θ = 300°

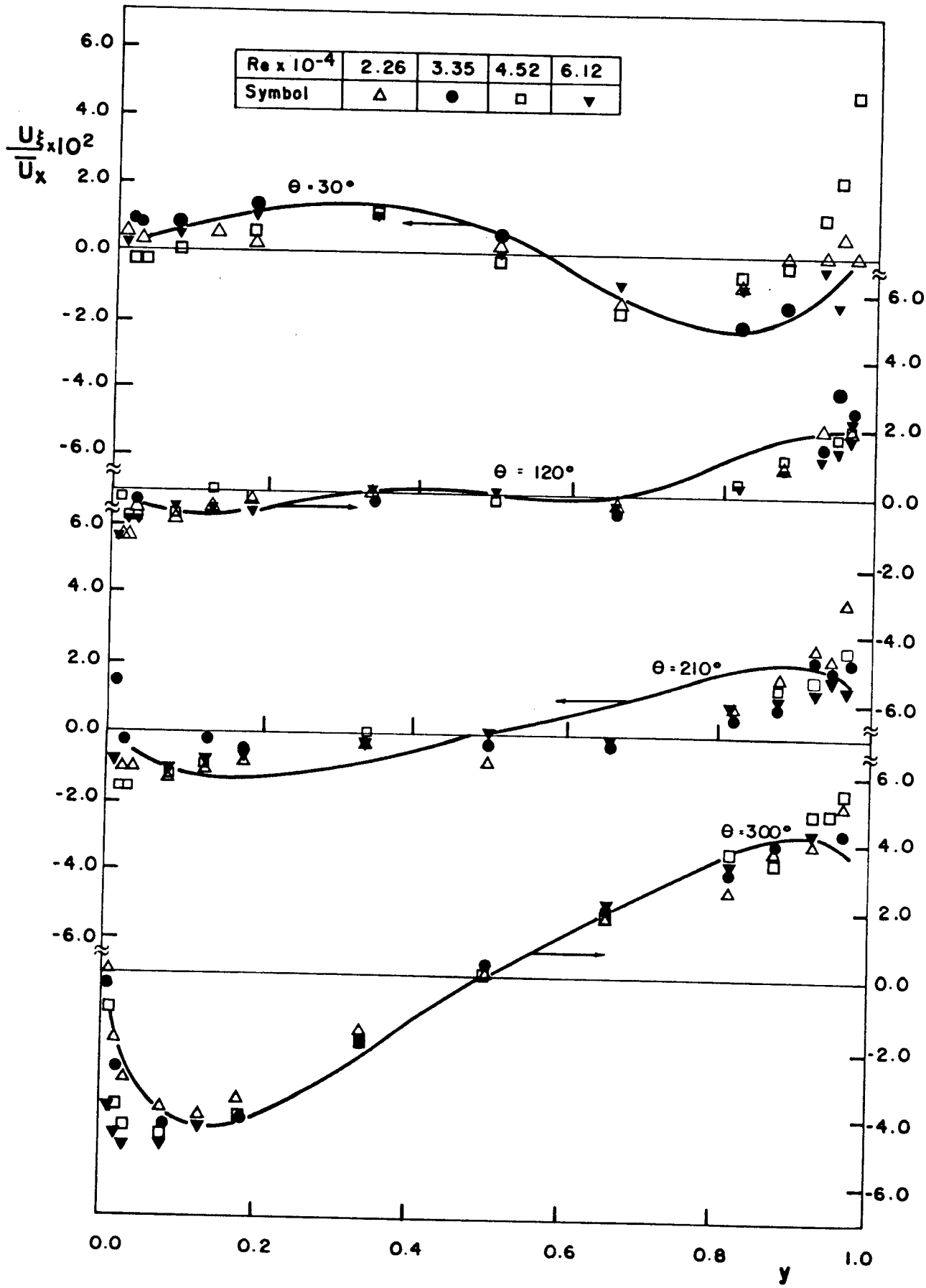

FIG. 16 - SECONDARY FLOW DISTRIBUTION

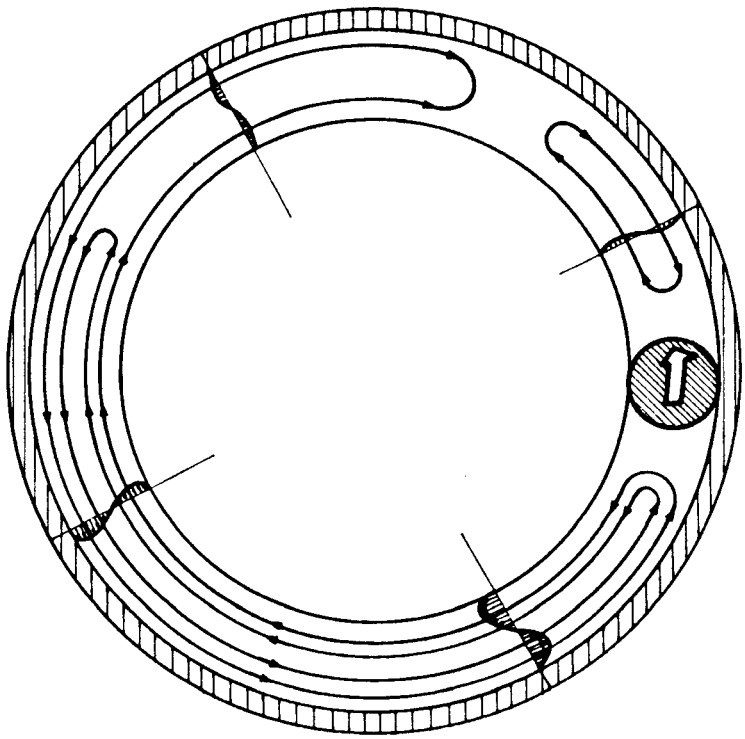

FIG. 17 - SECONDARY FLOW STREAMLINES

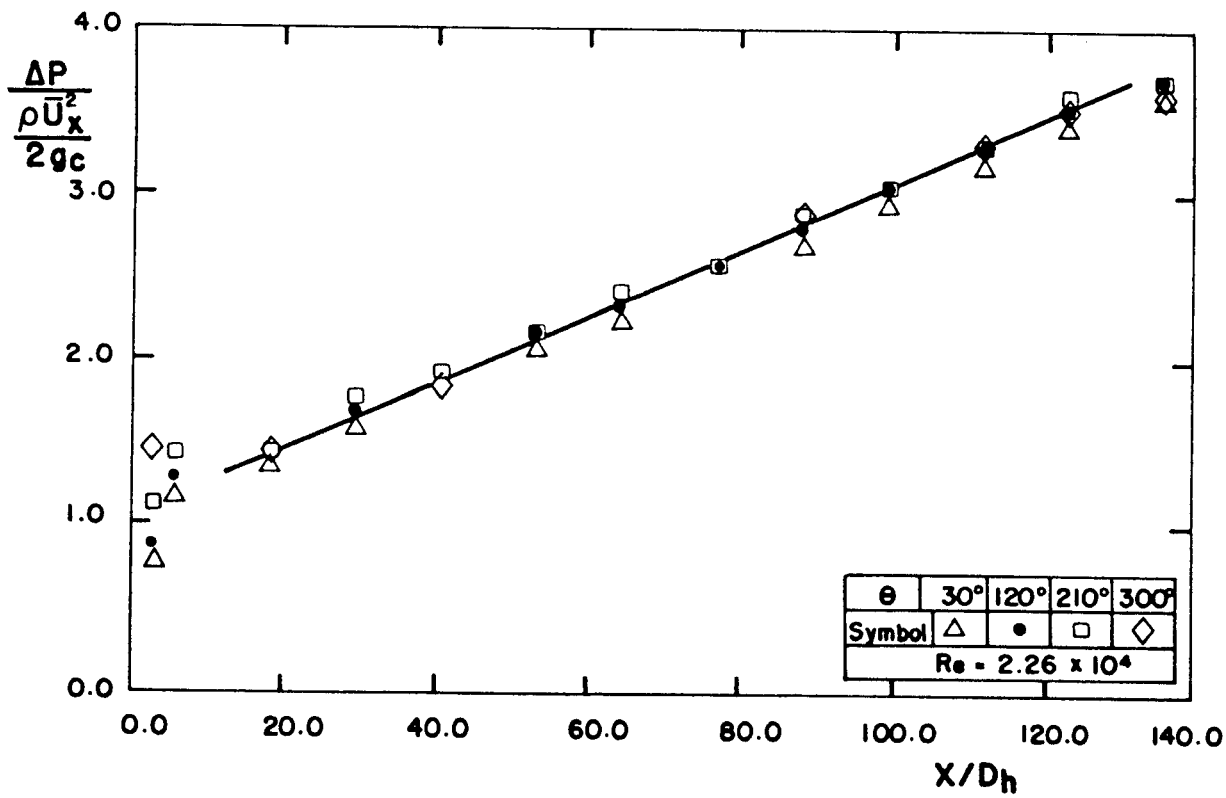

FIG. 18 - PRESSURE LOSS DISTRIBUTION RELATED TO PLENUM, Re = 22 600

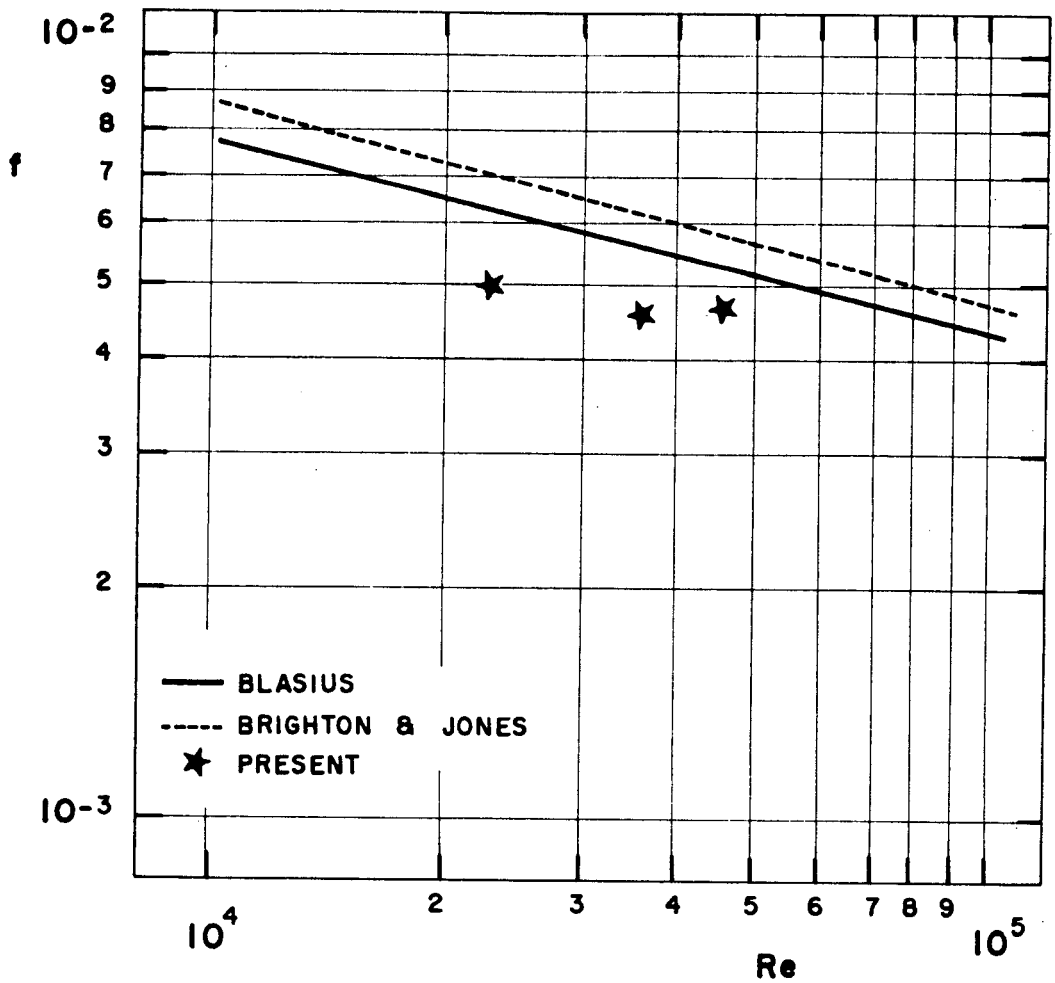

FIG. 19 - FRICTION FACTOR , f

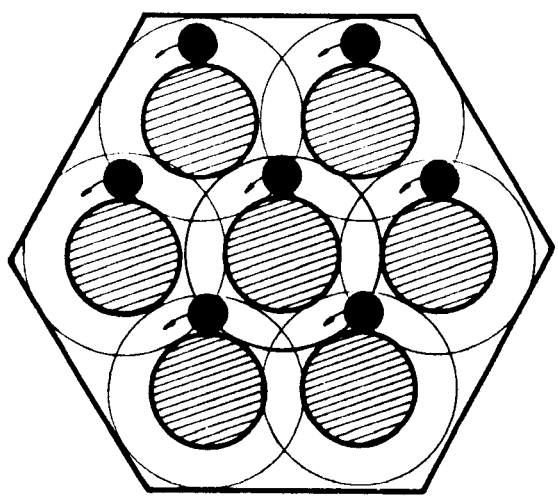

FIG. 20 - ANNULAR CHANNEL SUPERPOSITION MODEL